Impedance Based Resonance Analysis in a VSC-HVDC System

Ling Xu, *Student Member, IEEE,* and Lingling Fan, *Senior Member, IEEE*

***Abstract*—Resonances can limit power transfer in a Voltage Source Converter-High Voltage DC (VSC-HVDC) system. The objective of this paper is to develop impedance models for the rectifier AC system and the inverter AC system for a VSC-HVDC system. Resonance stability will be examined using Nyquist stability criterion and impedance frequency responses. The impedance models considers the outer control loop and the inner current control loops of VSCs. Impacting factors are then examined. Stability analysis demonstrates that the feed-forward filter, line length and power transfer level have significant impact on resonances. Time-domain simulation results obtained Matlab SimPowerSystems are used to validate the analysis.**

***Index Terms*—Admittance, impedance, resonance stability, VSC-HVDC.**

I. Introduction

VSC-HVDC is becoming an attractive solution to deliver renewable energy to main grids [1–3]. Harmonic resonances can impact the power quality and the power transfer level. Normally, harmonics generated by switching sequences could be eliminated by AC filters. However, there are low frequency harmonic resonances due to the interaction of AC grid and VSC controllers. Those resonances are not easy to be filtered out. Though harmonic resonances have been examined in VSC interfaced AC grids in [4–7], a comprehensive examination of the both AC systems (the rectifier side and the inverter side) has not been seen in the literature. It will be the objective of this paper.

Since harmonic resonances are related to electrical systems mainly, impedance or admittance model based analysis is feasible in understanding the phenomena. In [6–8], impedance models of grid-connected inverters are developed for resonance analysis. [6, 8] developed impedances models of converters with only the inner current control loops considered. The outer control loops are ignored. Investigation shows that grid inductor, shunt capacitor and phase locked loop (PLL) have impact on harmonic resonances.

Impedance models of the VSC converter with inner current control and outer DC/AC voltage control loops are developed in [7]. Resonance stability is studied for both power flow direction. The studied AC grid is represented by a series RL circuit. It is stated in [7] that for the interaction of a converter and the grid impedance, with outer loop ignored, instability cannot be detected. With the outer control loop and PLL considered, instability can be detected. Therefore, modeling of the outer control loops is important.

This work is supported in part by NSF ECCS grant # 1005277. L. Xu, and L. Fan are with Department of Electrical Engineering at University of South Florida, Tampa FL (Emails: lxu@mail.usf.edu and linglingfan@usf.edu).

In a VSC-HVDC system, there are two converters and each has its own control strategies. The rectifier controls power flow while the inverter controls DC-link voltage [9]. [7] studied only the interactions of the inverter and AC grid. The paper also assumes that the integral coefficients of converter proportional integral (PI) controllers are equal to zero. In many literatures, the integral gains are greater than the proportional gains [10, 11].

In this paper, resonance stability will be investigated for the two AC systems (the rectifier side AC grid and the inverter side AC grid). Typical VSC-HVDC controls will be adopted and impedance models of the systems will be developed with the inner and outer converter control loops included. Nyquist stability criterion and impedance frequency responses will then be applied to detect resonances. Impacting factors on stability such as feed-forward filter structure, line length and power transfer levels will be identified.

In the sections follow, the paper first describes the system topology of a VSC-HVDC system in Section II. The impedance and admittance models are presented. Analysis and simulations to evaluate resonances are carried out in Section III. The paper is concluded in Section IV.

II. System Model

A VSC-HVDC system is presented in Fig. 1, where the basic controller for the rectifier and inverter stations are also presented. Normally, power is sent from the rectifier station to the inverter station. Power control is implemented at the rectifier station, while the inverter station controls DC-link voltage to ensure power balance. An advantage of VSC-HVDC over Line-Commutated Converters HVDC (LCC-HVDC) is its reactive power compensation capability, which is provided by the reactive power controller or AC voltage controller.

For a balanced three-phase system, Fig. 2 shows the equivalent circuit of a VSC connecting with an AC grid via a coupling inductor L, where the resistor is neglected. The AC grid is modeled as an AC voltage source v_s with an impedance $Z(s)$. (1) describes the voltage and current relationship between grid and converter in time domain and represented in the dq frame. The letter with upper-line represents complex space vector, *e.g.*, $\overline{v} = v_d + jv_q$ and $\overline{i} = i_d + ji_q$. The angular speed within grid reference frame is ω_1, which is a constant throughout this paper.

$$L\frac{d\overline{i}}{dt} + j\omega_1 L\overline{i} = \overline{E} - \overline{v} \tag{1}$$

where E and v are the point of common coupling (PCC) voltage and the converter output voltage.

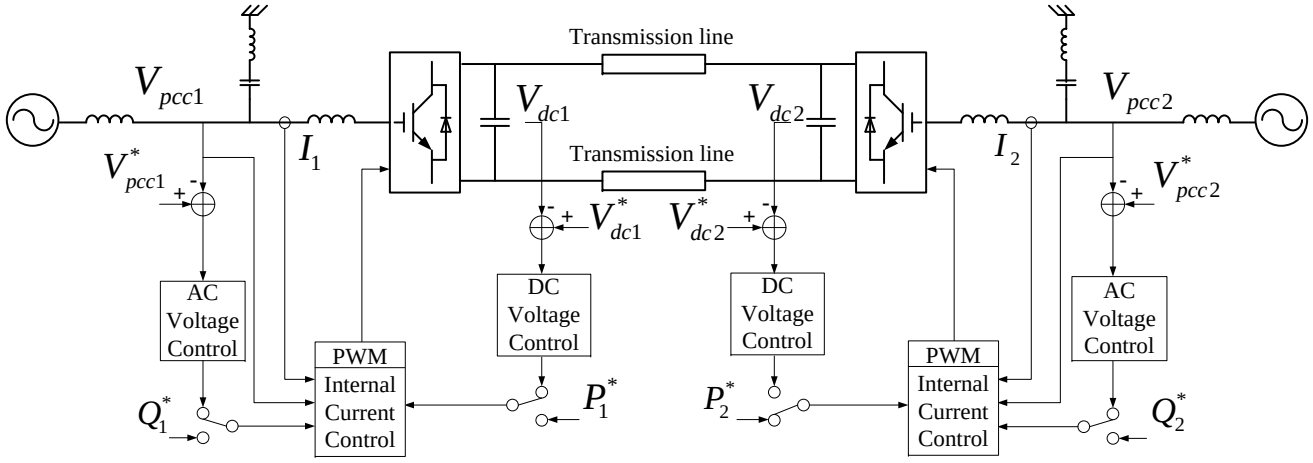

Fig. 1. A two-terminal VSC-HVDC system.

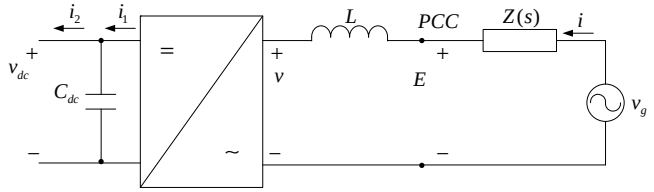

Fig. 2. Circuit model of a VSC and ac grid.

A. Impedance Models

1) Rectifier Station:

a) Current Control: The VSC-HVDC system consists of two terminal stations, one is the rectifier station and the other is the inverter station. Fig. 3 presents the controller of the rectifier station, in which active power P_{ref} and reactive power Q_{ref} are to be regulated.

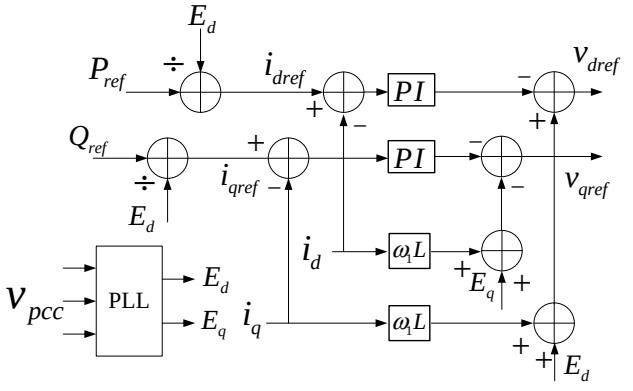

Fig. 3. Controller of the rectifier station.

Depending on the requirements of application, the reactive power control could be substituted with AC grid voltage control. v_{dref} and v_{qref} are the converter output voltages and could be derived as (2), which is essentially the inner current control loop.

$$\begin{aligned}\overline{v_{ref}} = &-(k_p + \frac{k_i}{s})(\overline{i_{ref}} - \bar{i}) - j\omega_1 L\bar{i} \\ &+ \frac{\omega_0^2}{s^2 + 2\xi\omega_0 s + \omega_0^2}\overline{E}\end{aligned} \tag{2}$$

The feed-forward items E_d and E_q are the PCC voltage measured in the dq frame and obtained through a filter. A second-order filter is included in (2), and the transfer function is shown in (3). Another option is first order filter, and the comparison of the two filters on resonance stability is conducted in Section III.

$$F_{2nd}(s) = \frac{\omega_0^2}{s^2 + 2\xi\omega_0 s + \omega_0^2} \tag{3}$$

where ω_0 is the cut-off frequency (1000 Hz) and ξ is the damping factor ($\frac{1}{\sqrt{2}}$).
The controller utilizes PI controllers:

$$F_c(s) = k_p + \frac{k_i}{s}. \tag{4}$$

Rearranging (2) leads to (5),

$$\overline{i^c} = g_c(s)\overline{i_{ref}} + y_i(s)\overline{E^c} \tag{5}$$

where

$$\begin{cases} g_c(s) = \frac{k_p s + k_i}{Ls^2 + k_p s + k_i} \\ y_i(s) = \frac{s^2(s + 2\xi\omega_0)}{(Ls^2 + k_p s + k_i)(s^2 + 2\xi\omega_0 s + \omega_0^2)} \end{cases} \tag{6}$$

(5) describes the relationship of the current $\overline{i^c}$ in terms of $\overline{i_{ref}}$ and $\overline{E^c}$. Alternatively, (5) could be written in matrix form (7).

$$\overline{\mathbf{i}^c} = \begin{bmatrix} g_c(s) & 0 \\ 0 & g_c(s) \end{bmatrix}\overline{\mathbf{i}_{ref}} + \begin{bmatrix} y_i(s) & 0 \\ 0 & y_i(s) \end{bmatrix}\overline{\mathbf{E}^c} \tag{7}$$

where $\mathbf{f} = [f_d, f_q]^T$ and f stands for current or voltage symbol.

b) Power Control: The rectifier station controls the active power transferred from the left-hand side grid to the converter, which is the outer control loop in dual dq control loops. Equation (8) computes the d axis current reference that controls the active power flow,

$$i_{dref} = \frac{P_{ref}}{E_d} = \frac{P_{ref}}{E_f} \tag{8}$$

where E_f is the d-axis PCC voltage after a filter.

$$E_f = F_{2nd}(s)\,|E| \tag{9}$$

The small signal representation of d axis current reference is then expressed as follows.

$$\Delta i_{dref} = -\frac{P_{ref}}{E_0^2} F_{2nd}(s) \Delta E_d \tag{10}$$

where E_0 is the rectifier PCC steady-state voltage. Since the direct reactive power compensation control is used throughout this paper, the q axis current reference can be derived similarly as above.

$$\begin{cases} i_{qref} = -\frac{Q_{ref}}{E_d} = -\frac{Q_{ref}}{E_f} \\ \Delta i_{qref} = \frac{Q_{ref}}{E_0^2} F_{2nd}(s) \Delta E_d \end{cases} \tag{11}$$

Combining (10) and (11) leads to (12).

$$\overline{\Delta i_{ref}} = \underbrace{\begin{bmatrix} -\frac{P_{ref\_rec}}{E_0^2} F_{2nd}(s) & 0 \\ \frac{Q_{ref}}{E_0^2} F_{2nd}(s) & 0 \end{bmatrix}}_{G_{Ei\_rec}(s)} \overline{\Delta E} \tag{12}$$

The input admittance of ΔE and Δi is then expressed as.

$$\begin{aligned} Y_{rec}(s) &= Y_i(s) + G_c(s) G_{Ei}(s) \\ &= \begin{bmatrix} y_i(s) - \frac{P_{ref}}{E_0^2} F_{2nd}(s) g_c(s) & 0 \\ \frac{Q_{ref}}{E_0^2} F_{2nd}(s) g_c(s) & y_i(s) \end{bmatrix} \end{aligned} \tag{13}$$

2) Inverter Station:

a) DC Voltage Control: The inverter station regulates the DC-link voltage and maintains the active power balance. The controller is depicted in Fig. 4, which consists of two control loops. The inner current control loop is identical to the rectifier station shown in Fig. 3, whereas the outer loop is replaced by a DC voltage controller. The DC voltage controller $F_{dc}(s)$ is a typical PI controller shown in (14).

$$F_{dc}(s) = k_{pdc} + \frac{k_{idc}}{s} \tag{14}$$

A feed-forward item $-P_{ref\_rec}/E_{d\_inv}$ is applied to improve the controller dynamic performance. Hence, the d-axis current reference could be established as follows.

$$i_{dref} = (k_{pdc} + \frac{k_{idc}}{s})(v_{dcref} - v_{dc}) - \frac{P_{ref\_rec}}{E_{d\_inv}} \tag{15}$$

The small signal model of the d-axis current reference is expressed in (16),

$$\begin{aligned} &i_{dref0} + \Delta i_{dref} \\ &= (k_{pdc} + \frac{k_{idc}}{s})(v_{dcref} - v_{dc0} - \Delta v_{dc}) - \frac{P_{ref\_rec}}{E_{d\_inv}} \end{aligned} \tag{16}$$

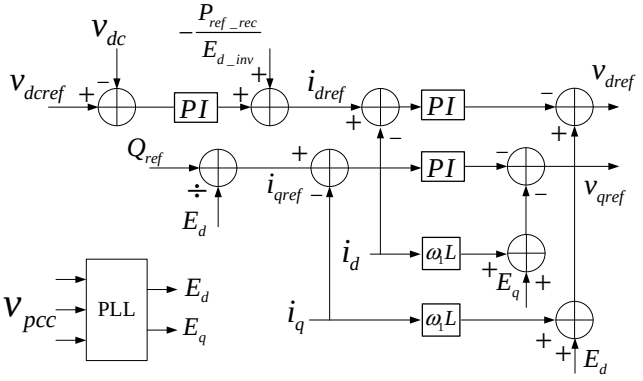

Fig. 4. Controller of the inverter station.

It can be assumed that $i_{dref0} = -P_{ref\_rec}/E_{d\_inv}$, since the active power delivered by inverter station is the same amount of rectifier station sent if power loss is neglected. The linear model (17) is then obtained.

$$\Delta i_{dref} = -\underbrace{(k_{pdc} + \frac{k_{idc}}{s})}_{F_{dc}(s)} \Delta v_{dc} \tag{17}$$

In order to derive Δv_{dc}, the complex power S has to be calculated.

$$\begin{aligned} S &= \left\{\overline{Ei}^*\right\} = (E_0 + \Delta E_d + j\Delta E_q)[i_{d0} + \Delta i_d - j(i_{q0} + \Delta i_q)] \\ &\approx E_0 i_{d0} + E_0 \Delta i_d + i_{d0} \Delta E_d + i_{q0} \Delta E_q \\ &+ j(-E_0 i_{q0} - E_0 \Delta i_q + i_{d0} \Delta E_q - i_{q0} \Delta E_d) \end{aligned} \tag{18}$$

The active power and reactive power will then extracted:.

$$\begin{cases} P = E_0 i_{d0} + E_0 \Delta i_d + i_{d0} \Delta E_d + i_{q0} \Delta E_q \\ Q = -E_0 i_{q0} - E_0 \Delta i_q + i_{d0} \Delta E_q - i_{q0} \Delta E_d \end{cases} \tag{19}$$

Assuming that $P_0 = E_0 i_{d0}$ and $Q_0 = -E_0 i_{q0}$, the small deviation parts of powers are then expressed in (20).

$$\begin{cases} \Delta P = E_0 \Delta i_d + i_{d0} \Delta E_d + i_{q0} \Delta E_q \\ \Delta Q = -E_0 \Delta i_q + i_{d0} \Delta E_q - i_{q0} \Delta E_d \end{cases} \tag{20}$$

Considering the dynamics on DC capacitor C_{dc}, the energy stored in the capacitor is

$$\begin{aligned} W &= \frac{1}{2} C_{dc} v_{dc}^2 \\ &\Rightarrow \frac{1}{2} C_{dc} \frac{dv_{dc}^2}{dt} = P_{dc} = P - P_L \\ &\Rightarrow C_{dc} v_{dc} \frac{dv_{dc}}{dt} = P - P_L \end{aligned} \tag{21}$$

where P_L is the active power consumed by load. Applying small perturbation leads to (22), the linear relationship between DC voltage and active power is obtained.

$$\begin{aligned} &C_{dc}(v_{dc0} + \Delta v_{dc}) \frac{d(v_{dc0} + \Delta v_{dc})}{dt} = P_0 + \Delta P - P_{L0} - \Delta P_L \\ &\Rightarrow C_{dc} v_{dc0} \frac{d\Delta v_{dc}}{dt} = \Delta P - \Delta P_L \end{aligned} \tag{22}$$

Since the current control loop of both inverter and rectifier station is identical, substituting (17) into (5) modifies equation (20) as:

$$\begin{aligned}\Delta P = E_0[-g_c(s)F_{dc}(s)\Delta v_{dc} + y_i(s)\Delta E_d] \\ + i_{d0}\Delta E_d + i_{q0}\Delta E_q\end{aligned} \tag{23}$$

Using (22) and (23), and assuming $\Delta P_L = 0$, Δv_{dc} is derived in terms of ΔE_d and ΔE_q.

$$\begin{aligned}&sC_{dc}v_{dc0}\Delta v_{dc} = -E_0 g_c(s)F_{dc}(s) + E_0 y_i(s)\Delta E_{d\_inv} \\ &+ \frac{P_0}{E_0}\Delta E_d - \frac{Q_0}{E_0}\Delta E_q \\ &\Rightarrow \Delta v_{dc} = \frac{(E_0^2 y_i(s) + P_0)\Delta E_d - Q_0 \Delta E_q}{sE_0 C_{dc} v_{dc0} + E_0^2 g_c(s) F_{dc}(s)}\end{aligned} \tag{24}$$

Substituting (24) into (17), Δi_{dref} could be represented in terms of ΔE_d and ΔE_q.

$$\begin{aligned}\Delta i_{dref} = &\underbrace{\frac{-(E_0^2 y_i(s) + P_0)F_{dc}(s)}{sE_0 C_{dc} v_{dc0} + E_0^2 g_c(s) F_{dc}(s)}}_{G_{dc}^d(s)} \Delta E_d \\ &+ \underbrace{\frac{Q_0 F_{dc}(s)}{sE_0 C_{dc} v_{dc0} + E_0^2 g_c(s) F_{dc}(s)}}_{G_{dc}^q(s)} \Delta E_q\end{aligned} \tag{25}$$

Besides DC-link voltage control, the inverter station could also compensate reactive power to the right-hand side grid, which utilizes the same control structure as that of the rectifier station. Therefore, the input admittance for the inverter station is shown in equation (26),

$$\begin{aligned}Y_{inv}(s) &= Y_i(s) + G_{Ei\_inv}(s)G_c(s) \\ &= \begin{bmatrix} y_i(s) + G_{dc}^d(s)g_c(s) & G_{dc}^q(s)g_c(s) \\ \frac{Q_{ref}}{E_0^2}F_{2nd}(s)g_c(s) & y_i(s) \end{bmatrix}\end{aligned} \tag{26}$$

where

$$G_{Ei\_inv}(s) = \begin{bmatrix} G_{dc}^d(s) & G_{dc}^q(s) \\ \frac{Q_{ref\_inv}}{E_{0\_inv}^2}F_{2nd}(s) & 0 \end{bmatrix}. \tag{27}$$

B. Stability Analysis

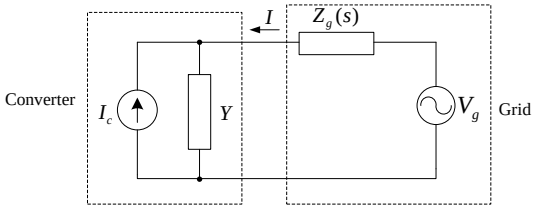

Fig. 5. Small-signal representation of a converter-grid system.

The grid is modeled as a combination of an ideal AC voltage source v_s and an impedance , which consists of a resistor R_g and an inductor L_g. Under dq frame, the impedance is expressed as $Z_g(s)$ in (28).

$$Z_g = \begin{bmatrix} R_g + sL_g & -\omega L_g \\ \omega L_g & R_g + sL_g \end{bmatrix} \tag{28}$$

Based on Fig. 5, the current I flowing from the grid to the converter is

$$I(s) = \frac{V_g(s) - Y^{-1}(s)I_c(s)}{Z_g(s) + Y^{-1}(s)} \tag{29}$$

which can be rearranged to

$$I(s) = [Y(s)V_g(s) - I_c(s)]\frac{1}{1 + Y(s)Z_g(s)} \tag{30}$$

Therefore, the stability analysis of the system relies on $Y(s)Z_g(s)$ in (30). Consequently, the grid-connected converter will operate stably if $Y(s)Z_g(s)$ satisfies Nyquist stability criterion. Since the VSC-HVDC system consists of a rectifier station and an inverter station, and the input admittance of each station depends on not only component parameters but also different control loops, it is obvious that many factors may affect the resonance stability.

III. Impacting Factors of Resonance Stability

In this section, we carry out frequency domain analysis based on impedance models and validate the analysis via Matlab/SimPowerSystems simulation. SimPowerSystems is a toolbox of Matlab/Simulink developed by Hydro-Québec of Montreal [12]. Models built in SimPowerSystems include switching details and are considered high-fidelity models. [13] compared the simulation results between SimPowerSystems toolbox and PSPICE, and demonstrated that SimPowerSystems is well suitable for the electrical circuits simulation containing switching devices because it can detect precise discontinuities.

In the literature, SimPowerSystems simulation results substituting experimental results are used for validation for VSC-HVDC systems. For example, [14] compared the simulations of CIGRÉ HVDC Benchmark System between SimPowerSystems and PSCAD/EMTDC, which demonstrated that both simulation tools are accurate and consistent during steady-state and transients situations. [15–17] investigated the various issues of VSC-HVDC using SimPowerSystems toolbox, including subsynchronous resonance, robust sliding-mode Controller, and Small-signal stability analysis.

Therefore, Matlab/SimPowerSystems simulation is also used as a tool to validate the impedance model based analysis.

A. Feed-forward Filter

The feed forward filter in the current control loop as shown in (3) has impact on the input admittance of rectifier $Y_{rec}(s)$ and hence can influence resonance stability. E_d and E_q are the feed forward PCC voltages in dq frame after the filter. In this subsection, the impact on stability of a second-order filter is compared with a first order filter. The transfer function of a first order low pass filter is as follows:

$$F_{1st}(s) = \frac{1}{s\tau + 1}. \tag{31}$$

where τ is the time constant (0.001 s.). Two scenarios with same power transfer level (100 MW) and same inverter control structures are examined:

- The feed-forward filter at the rectifier is a 1st order filter
- The feed-forward filter at the rectifier is a 2nd order filter

The line inductance L_g is chosen to be 0.05 H.

Figs. 6 and 7 present the real part of the total impedances for the rectifier side AC system and the inverter side AC system. Analysis of complex torque coefficients method in [18] indicated that the resonance frequencies are related to the roots of the real part of a transfer function. A brief explanation is offered as follows.

Assuming there are only oscillatory modes in the system, then $Z_g(s)+Z_{conv}(s)$ ($Z_{conv}=Y^{-1}$) should only have roots appearing as complex conjugate pairs ($-\sigma_l \pm \omega_l$). $Z_g(s)$ and $Z_{conv}(s)$ are rational functions. Therefore

$$Z_g(s)+Z_{conv}(s)=\frac{P(s)}{Q(s)} \tag{32}$$

where $P(s)$ and $Q(s)$ are polynomials of s

$$\begin{aligned} P(j\omega) &= \gamma\prod_l^n (j\omega+\sigma_l+j\omega_l)(j\omega+\sigma_l-j\omega_l) \\ &= \gamma\prod_l^n (\sigma_l^2+\omega_l^2-\omega^2+2j\sigma_l\omega) \end{aligned} \tag{33}$$

where γ is a constant.

Assuming negligible damping terms, then $P(j\omega)$ is a real function and denoted as $P_R(\omega)$. Hence

$$Re(Z_g(j\omega)+Z_{conv}(j\omega))=\alpha(\omega)P_R(\omega) \tag{34}$$

where $\alpha(\omega)$ is also a real function.

When $s=j\omega_l$, $P_R(\omega_l)\approx 0$, and hence $Re(Z_g(s)+Z_{conv}(s))\approx 0$. From the roots of the real part of the total impedances, resonance frequencies can be identified. For example, from Fig. 6, the resonance frequencies are 70 Hz and 190 Hz when 1st order filter or 2nd order filter is employed.

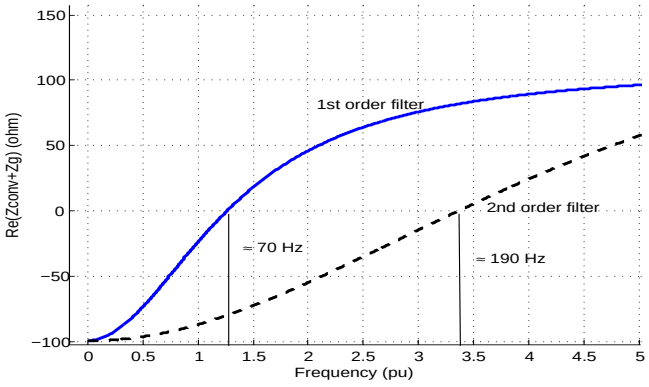

Fig. 6. Real part of the total impedance (left-hand side grid impedance plus converter impedance) at rectifier side.

A detailed VSC-HVDC model is built in Matlab SimPowerSystems to verify the analysis. The parameters of the system are listed in Appendix. The HVDC system is operated at 100 MW power transfer level. Fig. 8 shows the rectifier side d-axis current with two types of filters, where the oscillation frequency in the case of first-order filter is much lower than that when the 2nd -order filter case. Fig. 10 shows the active power at the rectifier side with two types of filter. Figs. 11 and 13 present the d-axis current and active power at the inverter side. Fig. 9 and Fig. 12 shows the d axis PCC voltage at rectifier and inverter stations with different filters. The d-axis PCC voltage with first order filter is lower than the d-axis PCC voltage with second order filter. Since the rectifier station operates on power control mode, which causes the d-axis current with first order filter case higher than the current with second order filter. The inverter station delivers active power transferred from rectifier station to right-hand side grid, therefore, the d-axis current with first order filter case is also higher than the second order filter case.

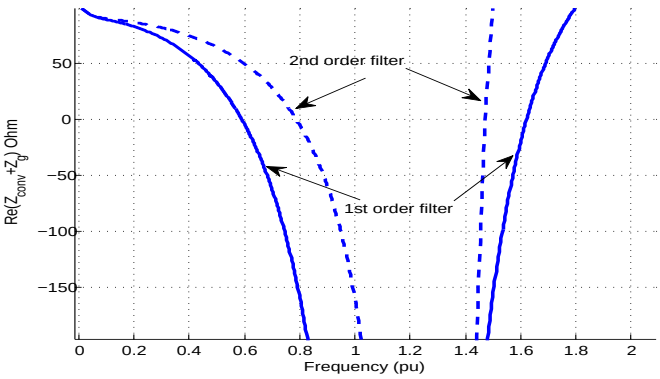

Fig. 7. Real part of the total impedance (right-hand side grid impedance plus converter impedance) at inverter side.

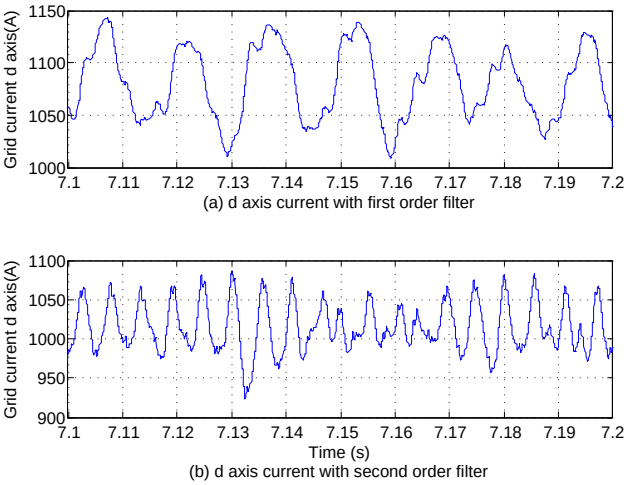

Fig. 8. Rectifier side d-axis current with different filters.

Figs. 8 and 10 show that the rectifier side AC system possesses a resonance around 70 Hz with 1st order filter and 190 Hz with 2nd order filter. This observation corroborates with the analysis in total impedance frequency responses in Fig. 6.

The inverter side AC system possesses at least two resonance frequencies as shown in Fig. 7 where two roots are iden-

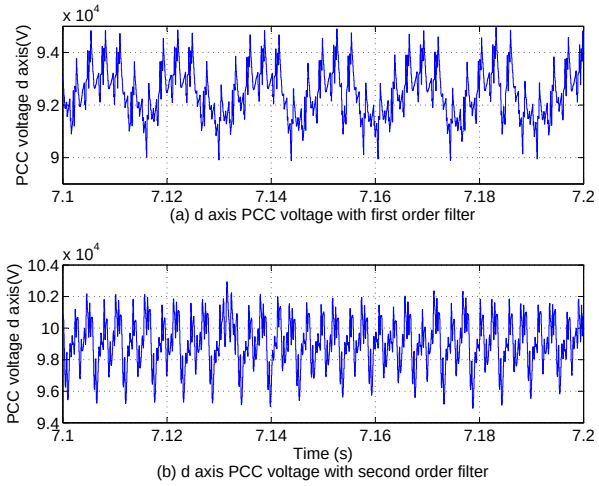

Fig. 9. Rectifier side d-axis PCC voltage with different filters.

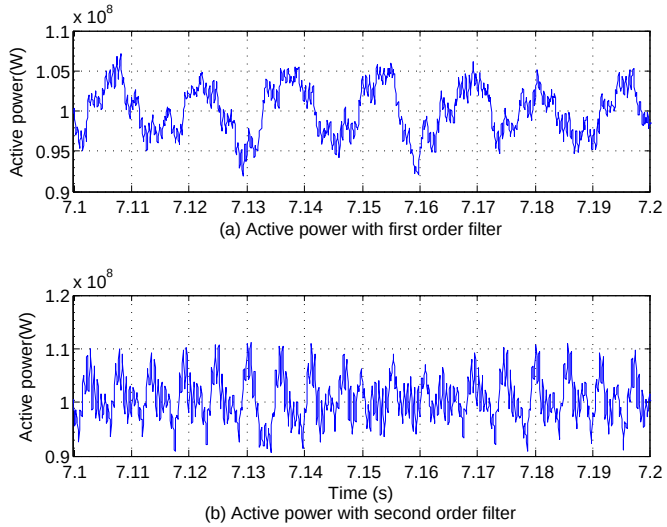

Fig. 10. Rectifier side active power with different filters.

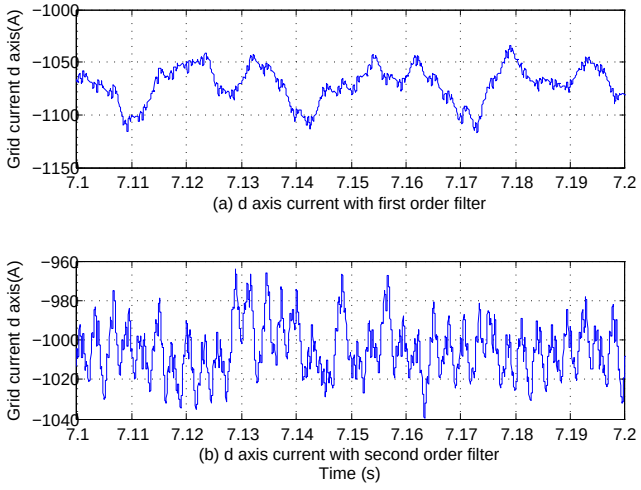

Fig. 11. Inverter side d-axis current with different filters.

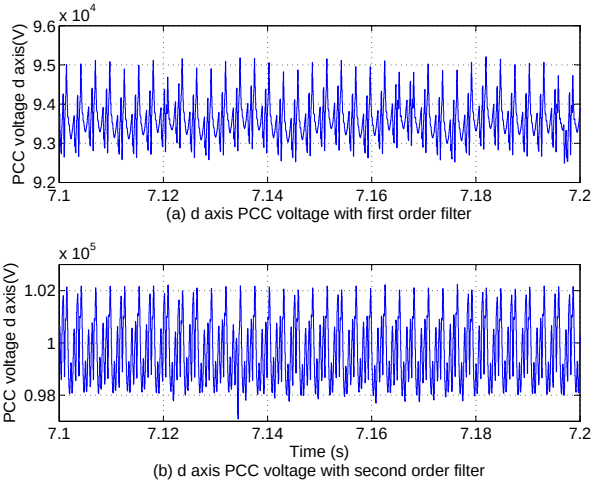

Fig. 12. Inverter side d-axis PCC voltage with different filters.

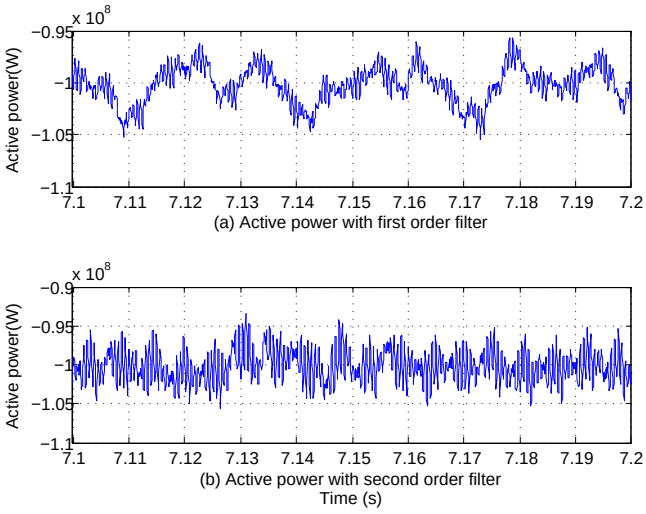

Fig. 13. Inverter side power with different filters.

tified. Simulation results also demonstrate more complicated waveforms in d-axis current and active power. The rectifier side AC line inductance is 0.02H while the inverter side line inductance is 0.012H. The resonances cause around 5% ripples in waveforms and do not pose stability issues.

B. AC Line Length

The impact of the line length of the rectifier AC side on resonance is studied in this subsection. The inductance of the rectifier AC system is varied to reflect the change of length. First-order feed forward filter is adopted in the current controller of the VSC. The power transfer level is set to 100 MW. The Nyquist curves for the eigenvalues of YZ_g are presented in Fig. 14.

The Nyquist curves shows that with the increase of line length, the more the system is prone to instability. Take the example of $L_g = 0.12H$, the time domain simulation results of the rectifier AC grid currents in dq-axis are shown in Fig. 15. It is clearly that the system has lost stability.

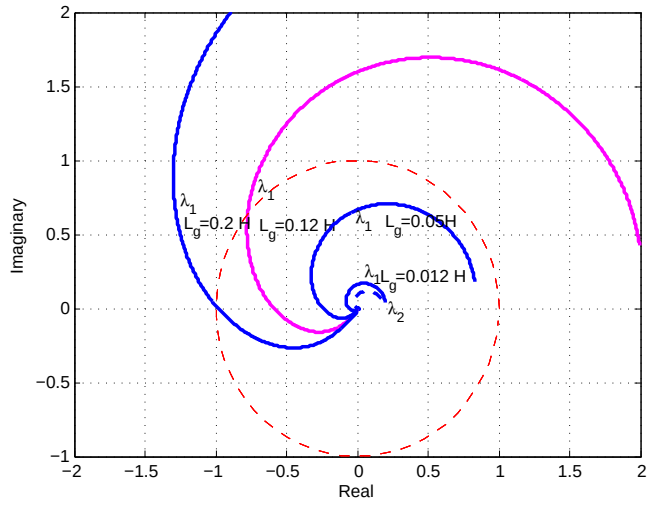

Fig. 14. Nyquist curves for the eigenvalues of YZ_g (rectifier ac system) for various line inductance.

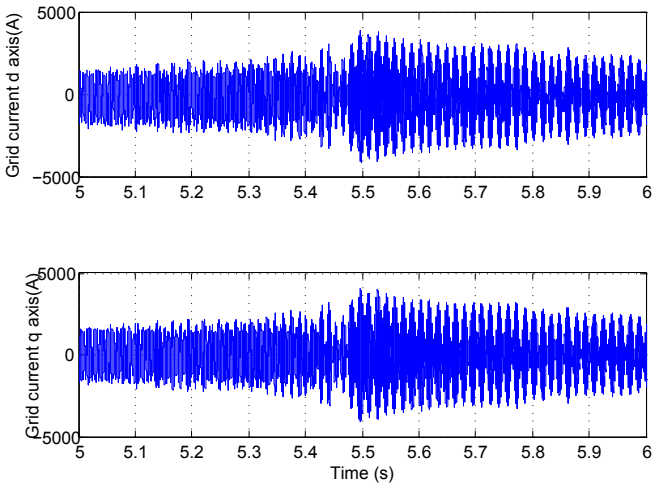

Fig. 15. Simulation results of i_d and i_q. $L_g = 0.05H$.

C. Power Level

Power transfer level is indicated in [7] to impact the converter impedance. Hence in this subsection, the impact of power level is investigated. Fig. 16 gives the Nyquist curves for one of the eigenvalues of YZ_g (rectifier AC system) for two power levels (100 MW and 170 MW). The line inductance is chosen to be 0.05 H. It is found from Nyquist curves that the higher the power transfer level, the more the system is prone to resonance.

The d-axis currents at the two power levels are shown in Fig. 17 and the active powers in the rectifier AC system at the two power levels are shown in Fig. 18. It can be observed that at 100 MW level, the ripple magnitude in i_d is about 5% of the mean magnitude, while it is more than 30% at 170 MW level.

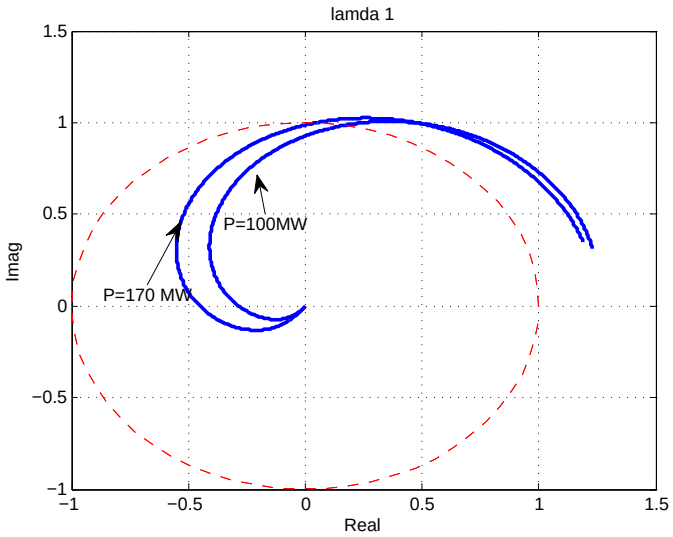

Fig. 16. Nyquist curves for the eigenvalues of YZ_g (rectifier ac system) for two power levels.

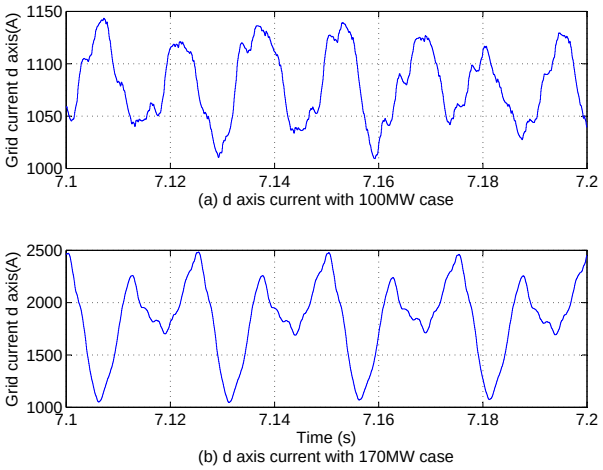

Fig. 17. d-axis current with different power level.

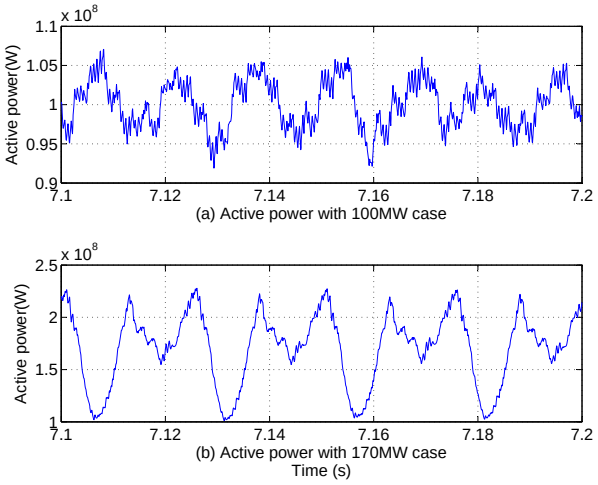

Fig. 18. Active power with different power level.

IV. Conclusion

Electrical resonances in a VSC-HVDC system is investigated in this paper. Frequency domain impedance models are developed for the rectifier side AC system and the inverter side AC systems. Nyquist stability analysis and impedance frequency responses are then applied to detect resonances. Impedance model based analysis demonstrates that the feed-forward filter, line inductance and level of power transfer have significant impact on resonance. A first-order filter leads to resonances with lower frequency compared to a second-order filter. Weak AC grid with long lines could lead to instability. The higher the power transfer level, the more obvious the resonances. Time-domain simulation results in Matlab/SimPowersystems using detailed models also demonstrate the impacting factors on resonances.

Appendix A

TABLE I
System Parameters of VSC-HVDC Model

Quantity	Value
AC system line voltage	100kV
AC system frequency	60Hz
Grid impedance	0.02H/0.012H
Grid filter capacity	18Mvar
Grid filter tuning frequency	1620Hz
DC rated voltage	250kV
DC cable parameters	0.0139Ω/km, 0.159mH/km, 0.231μF/km
DC cable length	20km

TABLE II
Parameters of Individual VSC

Quantity	Value
Switching frequency	1620Hz
Grid filter	0.04H
DC capacitor	96μF

TABLE III
Parameters of Controllers

Quantity	Value
Current controller	k_p=50, k_i=100
DC-link voltage controller	k_p=0.04, k_i=0.2

References

[1] N. Flourentzou, V. Agelidis, and G. Demetriades, "VSC-based HVDC power transmission systems: An overview," *IEEE Trans. Power Electron.*, vol. 24, no. 3, pp. 592 –602, Mar. 2009.

[2] K. Eriksson, "Operational experience of hvdc lighttm," in *Seventh International Conference on AC-DC Power Transmission*, Nov. 2001, pp. 205 – 210.

[3] L. Weimers, "Hvdc light: A new technology for a better environment," *IEEE Power Engineering Review*, vol. 18, no. 8, pp. 19 –20, Aug. 1998.

[4] M. Liserre, R. Teodorescu, and F. Blaabjerg, "Stability of photovoltaic and wind turbine grid-connected inverters for a large set of grid impedance values," *IEEE Trans. Power Electron.*, vol. 21, no. 1, pp. 263 – 272, Jan. 2006.

[5] J. Dannehl, C. Wessels, and F. Fuchs, "Limitations of voltage-oriented pi current control of grid-connected PWM rectifiers with LCL filters," *IEEE Trans. Ind. Electron.*, vol. 56, no. 2, pp. 380 –388, Feb. 2009.

[6] M. Cespedes and J. Sun, "Modeling and mitigation of harmonic resonance between wind turbines and the grid," in *IEEE Energy Conversion Congress and Exposition*, Sep. 2011, pp. 2109 –2116.

[7] L. Harnefors, M. Bongiorno, and S. Lundberg, "Input-admittance calculation and shaping for controlled voltage-source converters," *IEEE Trans. Ind. Electron.*, vol. 54, no. 6, pp. 3323 –3334, Dec. 2007.

[8] J. Sun, "Impedance-based stability criterion for grid-connected inverters," *IEEE Trans. Power Electron.*, vol. 26, no. 11, pp. 3075 –3078, Nov. 2011.

[9] A. Yazdani and R. Iravani, *Voltage-sourced converters in power systems : modeling, control, and applications*. Hoboken, N.J. : IEEE Press/John Wiley, 2010.

[10] S. Casoria, *VSC-Based HVDC Transmission System (Detailed Model)*. Natick, MA: The MathWork, Jan. 2010.

[11] J. Liang, T. Jing, O. Gomis-Bellmunt, J. Ekanayake, and N. Jenkins, "Operation and control of multiterminal hvdc transmission for offshore wind farms," *Power Delivery, IEEE Transactions on*, vol. 26, no. 4, pp. 2596 –2604, oct. 2011.

[12] MathWorks, "Electrical power systems simulation - simpowersystems - simulink," http://www.mathworks.com/products/simpower/index.html.

[13] L.-A. Dessaint, K. Al-Haddad, H. Le-Huy, G. Sybille, and P. Brunelle, "A power system simulation tool based on simulink," *Industrial Electronics, IEEE Transactions on*, vol. 46, no. 6, pp. 1252–1254, 1999.

[14] M. Faruque, Y. Zhang, and V. Dinavahi, "Detailed modeling of cigre hvdc benchmark system using pscad/emtdc and psb/simulink," *Power Delivery, IEEE Transactions on*, vol. 21, no. 1, pp. 378–387, 2006.

[15] N. Prabhu and K. R. Padiyar, "Investigation of subsynchronous resonance with vsc-based hvdc transmission systems," *Power Delivery, IEEE Transactions on*, vol. 24, no. 1, pp. 433–440, 2009.

[16] A. Moharana and P. Dash, "Input-output linearization and robust sliding-mode controller for the vsc-hvdc transmission link," *Power Delivery, IEEE Transactions on*, vol. 25, no. 3, pp. 1952–1961, 2010.

[17] G. Kalcon, G. Adam, O. Anaya-Lara, S. Lo, and K. Uhlen, "Small-signal stability analysis of multi-terminal vsc-based dc transmission systems," *Power Systems, IEEE Transactions on*, vol. 27, no. 4, pp. 1818–1830, 2012.

[18] A. Tabesh and R. Iravani, "On the application of the complex torque coefficients method to the analysis of torsional dynamics," *IEEE Trans. Energy Convers.*, vol. 20, no. 2, pp. 268–275, Jun. 2005.

Ling Xu is a Ph.D. candidate at University of South Florida. He received his Bachelor degree from Huazhong University of Science and Technology (Wuhan, China) in 2007 and his master degree from University of Alabama in 2009. His research interests include modeling and control of voltage source converter systems and real-time digital simulation.

Lingling Fan received the B.S. and M.S. degrees in electrical engineering from Southeast University, Nanjing, China, in 1994 and 1997, respectively, and the Ph.D. degree in electrical engineering from West Virginia University,Morgantown, in 2001.

Currently, she is an Assistant Professor with the University of South Florida, Tampa, where she has been since 2009. She was a Senior Engineer in the Transmission Asset Management Department, Midwest ISO, St. Paul, MN, form 2001 to 2007, and an Assistant Professor with North Dakota State University, Fargo, from 2007 to 2009. Her research interests include power systems and power electronics.